Mapping, Dynamics, and Future Change Analysis of Sundarbans Delta Using Cellular Automata and Artificial Neural Network Modeling

Hafez Ahmad, *Fellow, IEEE*, Felix Jose, and Darren James Shoemaker

***Abstract*—Over the past century, anthropogenic activities have had a significant impact on low-lying deltas. In this article, we utilized Landsat satellite images and sea-level data from the past thirty years to analyze the effects of land use/land cover (LULC) change, vegetation cover, and terrain temperature distribution on the Sundarbans delta. Anticipated LULC change has been simulated using a cellular automata algorithm coupled with an artificial neural network for 50 years into the future, considering climate change and other ecological drivers. The results of our analysis show that the thick, dense mangrove coverage in the Sundarbans has decreased from 65% in 1970 to 59% in 2020. However, the intricate network of channels has increased in width, and their coverage increased from 33% to 43% between 1990 and 2015. The simulations for 2030–2050 show that the mangrove coverage is expected to decline from 63.5% to 56.7% (a decrease of 628 km^2), while the total area of waterbodies will increase from 33.9% to 39.8%. By 2080, we predict that the mangrove coverage will decrease by about 269 km^2, the waterbodies will increase by 159 km^2, the built-up areas will increase by approximately 3.89 km^2, and the barren areas or beaches will cover 371 km^2 (3.9% of the total area). For the simulation of 2100, we predict that the mangroves will decrease by approximately 48% (4511 km^2). The waterbodies will increase to 45%, while the built-up areas and barren beaches will reach up to 117 and 517 km^2, respectively. There has been an increase in sea level in the Sundarbans by an average of +17.3, +9.6, + 6.1, +0.6, +1.6, and −4.01 mm/year at Khepupara, Charchanga, Hiron Point, Dladia, Diamond Harbor, and Sagar, respectively. The findings of this article can assist the Bangladesh and Indian governments and policymakers in developing optimal land use plans and implementing successful mangrove forest management and conservation plans in the future.**

***Index Terms*—Cellular automata algorithm coupled with an artificial neural network (CA-ANN), land use/land cover (LULC), QGIS, sea level rise, Sundarbans delta.**

I. Introduction

THE Sundarbans delta is a low-lying, dense mangrove forest, a natural coastal wetland shared by Bangladesh and India [1], [2]. Over 10 000 km of navigable tidal creeks ranging in size from a few meters to several kilometers crisscross the complex network of estuaries and islands within the delta [3]. The region's dynamic physiochemical conditions support a diverse range of flora and fauna, including extensive halophytic mangroves, making it a distinctive and ecologically rich environment [4]. This deltaic mangrove forest contains around 300 species of plants and 425 species of animals, including the endangered royal Bengal tiger, the Irrawaddy dolphin, crocodiles, and many other mangrove species [5]. It provides over 12 million people living nearby with ecosystem services, such as fisheries, forest products, climate regulation, water purification, ecotourism, erosion and flood control, and more [6], [7]. This deltaic forest serves as a nursery ground for aquatic species, protects coastal communities from natural disasters, stabilizes sea-land interactions, stores blue and sediments increases soil nutrients, and absorbs and removes pollutants before they enter the marine environment [8], [9], [10], [11]. The mangrove forest also reduces carbon dioxide emissions and is very effective in carbon sequestration. In addition to food, traditional medicine, firewood, and building materials, they help promote and sustain local biodiversity [9], [10].

The Sundarbans delta is primarily stable and of recent geologic origin, formed due to sediment deposition from the Ganges, Meghna, and Brahmaputra rivers, as well as numerous channels, creeks, and rivers in the Bengal basin, resulting from thousands of years of geomorphologic changes, tectonic movements in northwest Punjab, and the flow of the Ganges known as the Padma in Bangladesh [12]. Each year, these rivers discharge more than a billion tons of sediment into the Bay of Bengal (BoB), which serves as a conduit for sediment and freshwater from the Himalayas [13]. From May to September, the southwest monsoon delivers the most rainfall and sediment load to the Bengal coast [3]. Neotectonic motions in the Bengal basin between the 12th and 15th century AD also caused the basin to tilt eastward. Later, the merged Ganges and Brahmaputra Rivers once again flowed eastward to drain into Meghna in the middle of the 18th century. During the 16th century, the Ganges became eastward and joined the Brahmaputra. These activities continue to affect the deltaic basin's hydrological by altering deposition patterns and lowering freshwater imports regime [14], [15]. As a result, the delta construction method has mostly halted in the west, whereas it has augmented in the east. Between 1793 and 1870, the area of the Sundarbans increased by approximately

Manuscript received 18 October 2023; revised 14 December 2023 and 19 January 2024; accepted 13 February 2024. Date of publication 19 February 2024; date of current version 6 March 2024. *(Corresponding author: Felix Jose.)*

Hafez Ahmad is with the Department of Geosciences and Geosystems Research Institute, Mississippi State University, Mississippi, MS 39762 USA (e-mail: ha626@msstate.edu).

Felix Jose is with the Department of Marine & Earth Sciences, Florida Gulf Coast University, Fort Myers, FL 33965 USA (e-mail: fjose@fgcu.edu).

Darren James Shoemaker is with the Department of Wildlife, Fisheries, and Aquaculture, Mississippi State University, Mississippi, MS 39762 USA (e-mail: ds2951@msstate.edu).

Digital Object Identifier 10.1109/JSTARS.2024.3367116

800 km^2 [16], which is indicative of the high rate at which sediment was deposited. A study [17] showed that mangroves play a noteworthy role in the tidal shoal and the formation of a mainland. Throughout the Sundarbans mangrove forest, there are over 200 islands that are crisscrossed by more than 400 interconnected tidal waterways, making this the world's largest tidal mangrove forest.

Globally, mangrove forests are confronting a critical threat arising from a combination of anthropogenic and natural stressors. Anthropogenic stressors encompass coastal aquaculture, illegal wood cutting, and tourism, while natural stressors include cyclones, sea-level rise, and coastal erosion [18], [19], [20]. These factors are also the primary drivers of mangrove depletion worldwide. Specifically, tropical mangrove forests are vulnerable to sea-level rise, with an anticipated acceleration in the rate of relative sea-level rise to approximately 5 mm/year and 10 mm/year under low and high emission scenarios, respectively, by 2100 [21]. This rapid sea-level rise is expected to intensify mangrove forest loss and release significant carbon stores, exacerbating climate change [22]. One of the largest mangrove forests in the world, Sundarbans, lost about 20% of its land between 1980 and 2009, with waterbodies expanding by about 10%, posing a severe risk to national food security [23], [24]. Another assessment indicated a loss of about 3.8% between 1990 and 2019 [25]. The vanishing mangrove patches disrupt the transfer of biogeochemical materials between estuaries and coastal oceans, exacerbating climate change challenges [26]. Since the beginning of the 20th century, land use and land cover (LULC) patterns in the Sundarbans have changed dramatically. Various factors contributed to the rapid mangrove decline, including physical, climatic, and social factors, with human activities playing a substantial role [27]. The urgency of researching future LULC changes becomes evident when considering the Sundarbans delta's unique geographical characteristics. This Mangrove delta, marked by dynamic river distributaries, a monsoon-dominated climate, its inherently deltaic nature, and recent expansions in aquaculture, stands as an area particularly susceptible to natural disasters. Given these vulnerabilities, it is imperative to conduct a comprehensive analysis of the spatio-temporal patterns of LULC within this region, with a particular focus on preserving its invaluable mangrove habitats [28]. An ominous parallel can be drawn with the Chakaria mangrove forests, which have suffered from large-scale deforestation, extensive fishing within channels, growing human settlements, expansive shrimp farming, and intensive grazing [29]. The Sundarbans delta, should it continue to endure destructive anthropogenic activities, runs the perilous risk of mirroring the fate of the Chakaria mangrove forests [18], [30], [31]. Therefore, understanding and forecasting future LULC changes in the Sundarbans is not merely a research gap but an urgent imperative for the preservation of this unique and fragile ecosystem. The integration of the cellular automata algorithm with an artificial neural network (CA-ANN) presents a powerful approach for predicting future LULC changes. This combined model leverages the ability of CA to simulate spatial processes and transitions in LULC over time based on defined rules, while the ANN enhances the predictive capability by learning and recognizing complex patterns from historical data. Studies such as, [28], [32], [33], [34], [35] have demonstrated the effectiveness of this approach in various studies, such as the detection and prediction of LULC changes in different regions, including the use of CA-ANN for simulating LULC changes in specific urban areas and assessing past, present, and future LULC dynamics. Debanshi and Pal [36] also utilized CA-ANN to simulate the future deltaic landscape of the Ganges in terms of land-use changes for 2028 and 2038.

In this article, we aim to fill critical gaps in the existing knowledge by investigating the projected shift in LULC, land surface temperature (LST), and vegetation patterns within the Sundarbans delta. We will examine the repercussions of these changes, particularly in the context of sea-level rise and cyclone occurrences. The Sundarbans have experienced significant deforestation due to human activities and natural disruptions linked to climate and weather. Our study's uniqueness lies in its focus on the intricate interplay between LULC changes, sea-level rise, and cyclone events in this deltaic region. We hypothesize that the combined impact of these factors will have substantial effects on the Sundarbans delta's ecological and socioeconomic dynamics. Our primary objectives include modeling LULC changes, assessing their implications on the delta, and elucidating the complex relationships between sea-level rise, cyclones, and the region's vulnerability. By addressing these aspects, our research seeks to provide valuable insights for policymakers, conservationists, and researchers working to ensure the sustainable development and resilience of deltaic ecosystems. The objectives of this research are to: evaluate the spatio-temporal change of LULC, LST, and vegetation change from 1990 to 2020, and predict LULC for the years 2030, 2050, 2080, and 2100 using a CA-ANN model.

II. Methods and Materials

A. Study Area

The Sundarbans, situated within the GBM delta region, is the primary focus of this research. It spans from 21° 30' N to 22° 40' N and 88° 5' E to 89° 55' E, as depicted in Fig. 1. Geologically, this region has formed through the gradual deposition of silt by the GBM river system [37]. The region experiences a tropical monsoon climate with an average annual rainfall of 1800 mm [38], accompanied by temperature variations ranging from 11 °C to 37 °C [39]. A significant portion of this forest experiences daily tidal inundation with water levels influenced by the combined impact of ocean tides from the BoB and freshwater discharge from the rivers. In the monsoon season (June to September), the flow of freshwater increases, whereas during the dry season (October to May), freshwater input significantly diminishes due to the reduced water inflow from rivers. This extensive mangrove expanse is crisscrossed by numerous rivers, canals, and tidal creeks, giving rise to a dynamic network of mudflats and islands. The elevation of these landforms ranges from 0.9 to 2.11 m above sea level, with a land slope of 0.03 m [38], [40], [41].

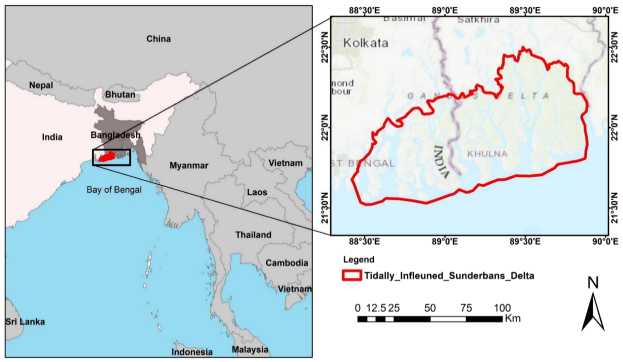

Fig. 1. Study area: The Sundarbans deltaic region straddling the boundary of India and Bangladesh is colored yellow on the map. Tide gauge stations are marked with red triangles.

TABLE I
DATA SOURCE: VARIABLE, DESCRIPTION, AVAILABILITY, AND REFERENCES FOR NDVI, LST, AND MEAN SEA LEVEL DATA ([42], [43], [44])

Variable	Tier Description	Availability	References
Images for LULC	Top of Atmospheric (TOA) Reflectance of Landsat 5-8 (Collection 1 Tier 1)	January 1984 to May 2022	[42]
LST and NDVI Image	TOA Reflectance from Landsat 5-8 (collection 1 Tier 1)	January 1984 to May 2022	[42]
Slope and elevation	NASA SRTM Digital Elevation 30m		[43]
Mean Sea level	Permanent Service for mean sea level	1937–2016	[44]

B. Data Collection and Processing

Landsat images (see Table I) from 57 and 8 missions were used in this article at intervals of 5 five years from 1990 to 2020. All processing, including atmospheric correction, cloud masking, clipping, calculation of normalized difference vegetation index (NDVI) and LST, and classification of LULC, was carried out in the cloud platform, Google Earth Engine (GEE). Annual Sea level data of tide Gauge stations of Sundarbans delta (1. Diamond harbor, 2. Haldia, 3. Khepupara, 4. Charchanga, 5. Hiron point, and 6. Sagar) was obtained from the website (https://www.psmsl.org/data/obtaining/stations/543.php)

C. Normalized Difference Water Index and Land Surface Temperature Calculation

NDVI [45], a dimensionless index depicting variations in vegetation reflectance between the visible and near-infrared spectra, is extensively used to assess changes in vegetation cover and crop health [46]. The ratio of the red to the near-infrared (NIR) band is used to generate an NDVI. Its range is from −1.0 to 1.0, mostly corresponding to green. Negative values are primarily water, and clouds, while values near zero are primarily composed of rocks and bare ground. Shrubs and meadows are represented by moderate values (between 0.2 and 0.3), while temperate and tropical forests are represented by big values (between 0.6 and 0.8). For Landsat 5/7/8, the formula is defined as follows [45]:

$$\text{NDVI} = \frac{(\text{Green band} - \text{NIR band})}{(\text{Green band} + \text{NIR band})}. \tag{1}$$

The LST is determined through a series of steps that encompass calculating brightness temperature (bt) from top-of-atmosphere reflectance, evaluating the proportion of vegetation, determining emissivity values, and finally, deriving the LST. Calculating bt from TOA reflectance from bands 10 and 6. This step was carried out by following the USGS website mentioned method [47]

$$\text{bt} = \frac{K2}{\ln\left(\frac{K1}{L_\lambda} + 1\right)} - 273.15 \tag{2}$$

where $K1$ is the thermal conversion constant, $K2$ is also the thermal conversion constant, and L_λ is TOA reflectance. $K1$ and $K2$ can be found in metadata.

Quantification of the proportion of vegetation: According to [48], the proportion of vegetation was quantified

$$P_v = \left(\frac{\text{NDVI} - \text{NDVI}_{\min}}{\text{NDVI}_{\max} - \text{NDVI}_{\min}}\right)^2. \tag{3}$$

Quantification of the error correction (the value of emissivity): Emissivity was calculated as follows [44]:

$$E = m * P_v + n \tag{4}$$

where m is the vegetation's emissivity value, which in this instance was 0.004. n is the soil emissivity value, which in this instance was 0.986.

Calculating LST: Brightness temperature to actual LST was calculated as follows [49], [50]:

$$\text{LST} = \frac{bt}{1 + \left[\left(w * \frac{bt}{p}\right) * \ln(E)\right]} \tag{5}$$

where $w =$ length of the emitted radiation (band 10), in this case, 0.00115 was used, $p =$ constant value obtained from $h*c/\sigma$ is $1.438*10^{-2}$ mk here h is the plank's constant ($6.626*10^{-34}$), c is the velocity of light ($3*108$ m/s), and s is the Boltzmann constant ($1.38*10^{-23}$ J/K).

D. LULC Change Detection, Image Classification and Modeling

The LULC change detection method is a powerful tool for assessing changes in change of the LULC over time, including the amount of loss and gain, characteristics, and patterns. It also assists with natural resource management, utilization, and decision-making related to using natural resources and the environment [31], [34]. The use of remote sensing (RS) data for spatiotemporal analysis has grown in prominence due to its repetitive acquisition, making it a valuable resource for accurate LULC detection and mapping [32], [33]. With the capacity to process RS data in cloud-based platforms like the GEE, the field has gained powerful tools to efficiently analyze and understand landscape changes. In the GEE for satellite image classification, TOA images were used instead of surface reflectance (SR) images due to the limited availability of SR images. The random

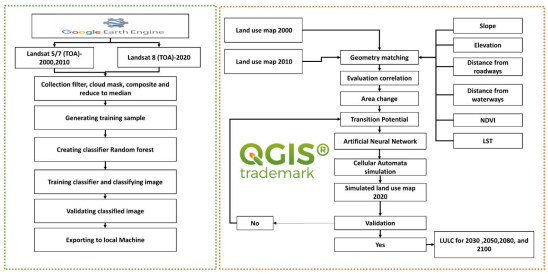

Fig. 2. Methodology for image collection processing, classification, accuracy assessment, and simulation for the future. The green box represents image classification and the orange box represents the CA-ANN modeling and simulation scheme.

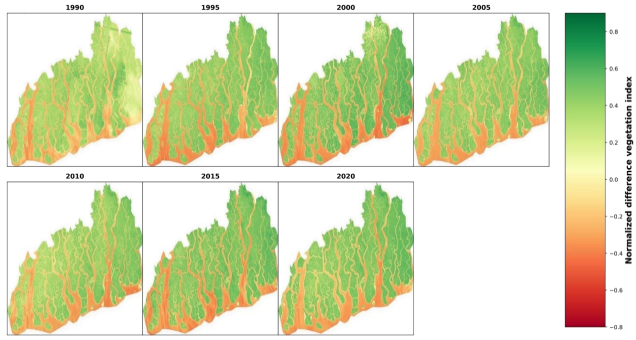

Fig. 3. Vegetation distribution from 1990 to 2020. Here, NDVI 0.1 to +1 denotes Vegetated areas, 0 denotes bared land, and −0.1 to −1 denotes waterbodies.

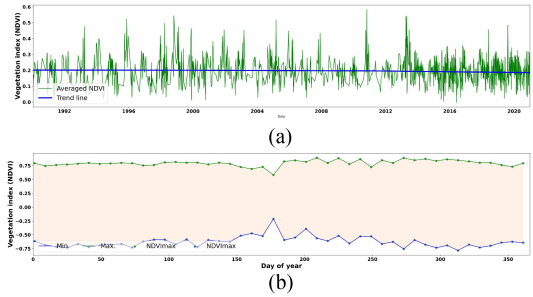

Fig. 4. Historical NDVI plot for the Sundarbans. (a) Time series with the blue-colored regressive trend and green-colored line plot of LST from 1990 to 2020. (b) Daily times with maximum and minimum NDVI daily average of a year.

forest (RF) machine learning algorithm was used on the GEE platform for image classification. Breiman [51] first proposed RF as an ensemble learning method that consists of many decision trees. RF assigns classification labels to many decision trees. For an explicit explanation of the RF classifier, the readers are directed to [51]. This combines a collection of randomized trees. The bagging approach replaces training samples with a subset of training samples. The same sample can be selected multiple times, while others may not. LULC has been quantified using RF in RS multispectral image classification [48], [52], [53], [54]. The GEE platform's built-in RF algorithm was applied for image classification based on four major classes including mangrove patches, barren land, built-up areas, and waterbodies.

There are various simulation techniques available for predicting future land cover changes, such as Markov chain, cellular automata, logistic regression, and artificial neural networks [55], [56]. A particularly noteworthy approach is a CA-ANN generates multiple output neurons to simulate multiple land-use changes nonlinearly [57]. An advantage of the CA-ANN model is that it can record intricate nonlinear aspects throughout modeling operations and provide insight into the transition rule for the underlying LULC pattern. Research has confirmed that CA-ANN can be effectively used to generate future LULC predictions with higher accuracy [28], [32], [33], [34], [55]. With the MOLUSC [58] plugin of QGIS [59], future LULC could be predicted using a CA-ANN model. This model uses elevation, slope, and, as a land-use factor, distances from major roadways and waterways. The Euclidean distance tool in ArcGIS [60] was utilized to determine the distance from the waterways (canal, ditch, streams, drain, streams, rivers, and channels). The model uses two LULC rasters from two periods as dependent variables and independent variables, including elevation, slope, and the distance from major highways as land-use factors. To evaluate conversion metrics and change probabilities, two variables were used as inputs. ANN model was then used to predict the transition potentials of LULC changes. Finally, simulated rasters were derived based on these using CA. For example, classified images of 1990, 2000, and 2010 were used to predict the LULC of 2020 then, the predicted 2020 images were validated with the classified 2020 images. LULCs for 2030, 2050, 2080, and 2100 were simulated with acceptable results and accuracy (see Fig. 2). The mathematical equation for the CA model is written as follows:

$$S(t, t+1) = f(s(t), N. \tag{6}$$

Here, S $(t+1)$ denotes the condition of the system at the moment $(t, t+1)$. Based on a bottom-up method, this technique analyzes accurate models of urban growth and LULC processes [58].

E. Accuracy Calculation

Calculating accuracy is crucial when classifying images. Information derived from RS data is evaluated in terms of its accuracy. For this purpose, labeled data has been split into 70% as training and 30% as testing set for each mentioned year. Based on this, major accuracy assessment matrices such as validation overall accuracy, producer, user, and kappa coefficient were calculated. We primarily employed commonly available methods for assessing the accuracy of image classification to assess the results[48], [52], [61], [62], [63].

A. Vegetation and LST Distribution

The daily NDVI ranged from −1 to 1, with an average of 0.2. NDVI widely varied across the delta (see Fig. 3). The highest and lowest NDVI was found in October, January, May, December, and February because this is a tidal-influenced mangrove delta. It is fascinating that the maximum NDVI is not consistently found across all areas simultaneously. However, Fig. 4 shows an overall decreasing trend line from 1990 to 2020.

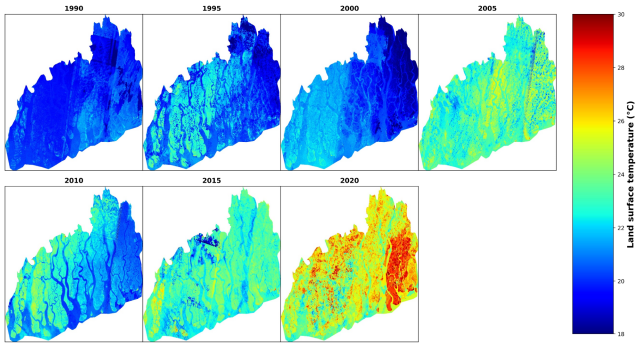

Fig. 5. LST distribution from 1990 to 2020.

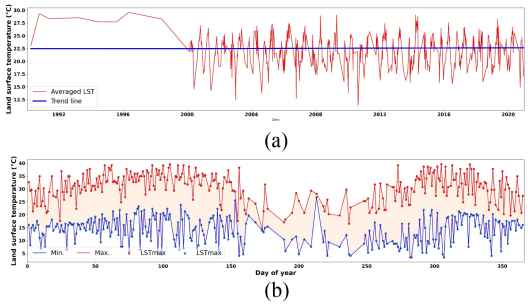

Fig. 6. Historical LST plot for the Sundarbans delta from 1990 to 2020. (a) Time series with the blue-colored regressive trend and red-colored line plot of LST from 1990 to 2020. (b) Daily times with maximum and minimum LST daily average of a year.

It should be noted, however, that the average minimum from 1990 to 2020 NDVI for all months is not equal, ranging from −0.72 to 0.85. November represents the lowest negative NDVI (−0.716), whereas June represents the least low negative NDVI (−0.48). This negative NDVI mostly indicates inundation extent and magnitude across the Sundarbans delta. But still, July to November also shows the highest vegetated (≥0.81) areas. For 1990–2000, 2000–2010, and 2010–2020, we calculated average NDVIs as 0.19, 0.20, and 0.19, maximum NDVIs as 0.84, 0.78, and 0.79, and minimum NDVIs as −0.73, −0.66, and −0.64 respectively (see Fig. 4).

On the other hand, For the Sundarbans delta, thirty years of LST showed a huge temperature fluctuation from 3 °C to 39 °C, with an average of 22 °C (see Fig. 5). Most of the warmest months were April, November, and February, with maximum LSTs exceeding 39 °C for the period 2010–2019. In contrast, some delta areas experienced the lowest LSTs, around 3.5 °C in October, November, August, and December (see Fig. 6) used.

The average maximum LST in March–May month from 1990 to 2020 ranged from 31.6 to 29 °C, while the average lowest LST in June to September ranged from 9.8 to 14 °C. The mean LSTs for 1990–2000, 2000–2010, and 2010–2020 were 23.6 °C, 22.3 °C, and 22.7 °C, maximum LSTs were 29.4 °C, 28.3 °C, and 29.40C, and minimum LSTs were 18 °C, 16.5 °C, and 17.6 °C (see Fig. 6) used.

B. Accuracy Analysis

For the accuracy analysis, 70% of the data was used for training, while 30% was used for testing. Most accuracy, whether user or producer, accuracy percentages range from 100%–85% for the mangrove and 100%–79% for the waterbodies. The accuracy of built-up areas is 0 in 1990, 1995, and 2010 because we did not identify this class type for these years.

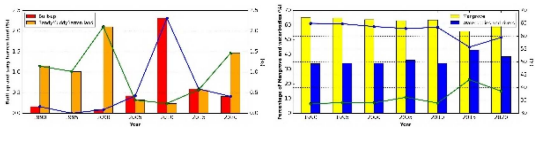

Fig. 7. Percentage of LULC classes from 1990 to 2020 in the Sundarbans delta.

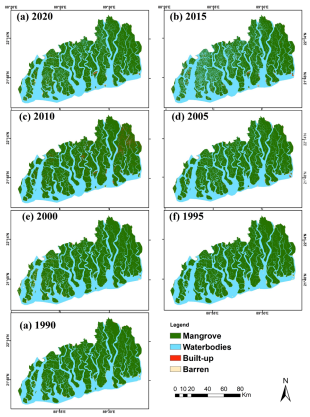

Fig. 8. LULC map for the Sundarbans delta from 1990 to 2020. The first image starts with 1990, and the last image of LULC for 2020.

C. Patterns of LULC Changes and Transition Analysis

LULC in the Sundarbans delta from 1990 to 2020 was quantified using Landsat imagery and an RF model within the GEE platform, encompassing categories such as mangrove forests, waterbodies, built-up areas, and barren lands. As mangroves mainly cover the delta, this class always dominated the LULC classes. The mangrove forest occupied 6090 km^2, which was 65% of the entire Sundarbans delta, 33% was waterbodies, and 1% was barren land in 1990 (see Fig. 7). In 1995, the mangrove area decreased slightly to 64%, and the area of waterbodies increased; while barren land, remained the same. By the year 2000, the mangrove coverage had changed slightly, while the waterbodies expanded significantly and the barren land had increased to about 2%, which means 198 km^2. In 2005, mangroves again had the same reduction rate, higher water rate, and no significant change. From 2005 to 2010, the mangroves increased significantly, and the waterbodies shrunk from 36% to 34%, and buildup area of 2.3%. From 2010 to 2015, mangroves significantly decreased by about 7% over the previous year, and much of the waterbodies were probably flooded. Waterbodies were 43%, but barren land and human settlement appeared slightly lower in the image (see Fig. 8). The canopy of mangrove forests varied from 65% to 55% over the study periods, whereas the coverage of waterbodies, including rivers and channels, varied from 33% to 43%, and the spatial extent of other LULC classes never exceeded 2%. It is evident that mangrove coverage has decreased over the years; its coverage in 1970 was 65%, and in

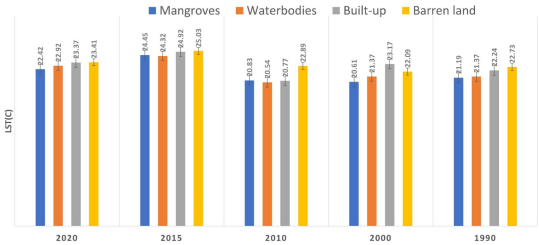

Fig. 9. LULC class-wise LST distribution. 1990–2020.

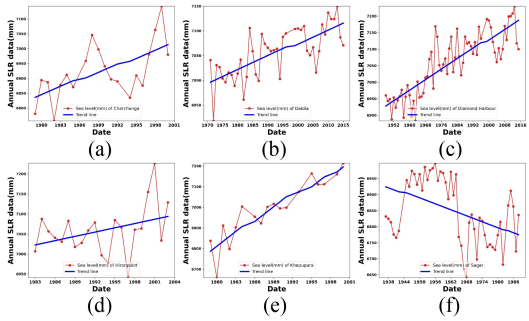

Fig. 10. Sea level data from six tide gauge stations near or within the Sundarbans delta. The a–f denotes Charchanga, Daldia, Diamond Harbour, Hiron Point, Khepupara, and Sagar respectively.

2020, it became 59%. In contrast, waterbodies were increasing in the area; their coverage was 33% in 1990, and it became 38% in 2020, mainly 43% in 2015 (see Figs. 7 and 8).

D. Class Wise LST Distribution

In 1990, all LULC classes had similar LSTs ranging from 21.1 °C to 22.7 °C. The barren land had the highest temperature (22.7 °C), and mangroves had the lowest (21.1 °C). The average LST for the barren, built-up, mangrove, and waterbodies classes in 2000 was 22.1 °C, 23.2 °C, 20.6 °C, and 21.4 °C, respectively. LSTs in 2010 varied slightly between 20.5 °C and 22.9 °C across all LULC classes. The barren land had the highest temperature (22.9 °C), and the waterbodies had the lowest (20.5 °C). The average LSTs for the barren land, built-up, mangroves, and waterbodies classes in 2020 were 23.4 °C, 23.37 °C, 22.4 °C, and 22.9 °C, respectively (see Fig. 9).

E. Sea Level Data Analysis

Six tide gauge historical sea-level visualization is shown in Fig. 10, except for Sagar, and the other four stations show rapidly rising sea levels. The linear trend line of Charchnaga, Hiron Point, Daldia, Diamond Harbor, and Khepupara is positive. According to the PSMSL data, sea levels were rising by an average of +17.294, +9.605, + 6.1, +0.571, +1.549, and −4.01 mm/year in Khepupara, Charchanga, Hiron Point, Daldia, Diamond Harbor, and Sagar, respectively. Khepupara and Hiron Point are inside Sundarbans Forest, and their rising sea level recording shows an alarming trend and rate.

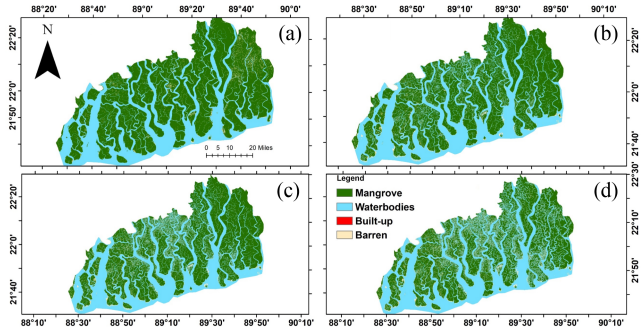

Fig. 11. Simulation of LULC for the Sundarbans delta from 2030 to 2100. Here, labels (a) indicate 2030, (b) denote 2050, (c) indicate 2080, and (d) indicate 2100.

F. Simulated LULC

By 2020, the total area covered by mangrove vegetation was 5573 km^2, which is about 60% of that year, and later in the simulation, it increased slightly to 5948 km^2. Barren land, which now covers 1.4% of the area (114 km^2), has seen a substantial reduction. Interestingly, the simulation of 2030–2050 shows a slightly reverse picture of mangrove coverage declining from about 63.5% to 56.7% (a decrease of 628 km^2), while waterbodies are gradually getting larger according to the previous trend, many mangrove areas would be flooded, and the total area of waterbodies has increased from 33.9% to 39.8%. It is a wonder that the built-up areas will decrease in 2050, whereas barren land will increase by almost 2.6%. By 2080, the mangrove coverage will decrease by about 269 km^2, waterbodies will increase by 159 km^2, but the built-up areas will increase by about 3.89 km^2, and barren land will become 371 km^2 (3.9% of the total area). In the present LULC simulation of a 2100-year, the mangrove forest areas would be decreased by about 48% or 4511 km^2. The waterbodies increased up to 45%, and the built-up areas and barren land reached 117 and 517 km^2 (see Fig. 11).

IV. Discussion

In this article, we analyzed three decades of spatio-temporal vegetation and land surface data, in addition to predicting LULC changes up to the year 2100 using CA-ANN. The vegetation analysis showed that there was still a wide variation in the NDVI values because barren or sandy shores have very low NDVI values due to tides, which are flooded twice daily in the mangrove [64] and less NIR reflectance during high tide due to the presence of seawater [19]. Our findings underscore a concerning trend where waterbodies are encroaching upon the mangrove forest, with mangrove coverage in the Sundarbans delta decreasing from approximately 65% to 59% (see Table II, Figs. 7 and 8). This phenomenon may be attributed to rising sea levels and deforestation [3], [65], [66] via overexploitation and illegal fire-cutting [18]. Over the last three decades, the Sundarbans' surface water temperature has increased by about 0.5 °C per decade. The mean summer temperature of Sundarbans is expected to rise by 1.5 °C–2 °C, while the average winter temperature is expected to rise by 2.5 °C to 3 °C by 2050, which can cause sea level to rise more rapidly [67]. For low to high

TABLE II
LULC YEAR-WISE COVERAGE, CHANGE, PERCENTAGE OF THE YEAR, AND PERCENTAGE OF CHANGE

	1990	1995	Change	1990%	1995%	% change
Mangrove	6090.76	6073.19	−17.57	65.0	64.8	−0.18
Waterbodies	3155.65	3200.63	44.98	33.7	34.2	0.48
Built-up	15.28	0.18	−15.1	0.2	0.0	−0.16
Barren	107.53	95.22	−12.31	1.1	1.0	−0.13
	1995	**2000**	**Change**	**1995 %**	**2000 %**	**% change**
Mangrove	6073.19	5974.63	−98.56	64.8	63.8	1.05
Waterbodies	3200.63	3189.14	−11.49	34.2	34.0	−0.12
Built-up	0.18	8.28	8.1	0.0	0.1	0.09
Barren	95.22	197.18	101.95	1.0	2.1	1.09
	2000	**2005**	**Change**	**2000 %**	**2005 %**	**% change**
Mangrove	5974.63	5903.8	−70.82	63.8	63.0	0.76
Waterbodies	3189.14	3395.64	206.5	34.0	36.2	2.20
Built-up	8.28	39.66	31.38	0.1	0.4	0.33
Barren	197.18	30.12	167.06	2.1	0.3	−1.78
	2005	**2010**	**Change**	**2005 %**	**2010%**	**% change**
Mangrove	5903.8	5948.02	44.21	63.0	63.5	0.47
Waterbodies	3395.64	3182.1	−213.54	36.2	34.0	−2.28
Built-up	39.66	216.55	176.89	0.4	2.3	1.89
Barren	30.12	22.56	−7.56	0.3	0.2	−0.08
	2010	**2015**	**Change**	**2010%**	**2015%**	**% change**
Mangrove	5948.02	5223.98	−724.04	63.5	55.8	−7.73
Waterbodies	3182.1	4035.9	853.8	34.0	43.1	9.11
Built-up	216.55	55.64	−160.91	2.3	0.6	−1.72
Barren	22.56	53.71	31.15	0.2	0.6	0.33
	2015	**2020**	**Change**	**2015%**	**2020%**	**% change**
Mangrove	5223.98	5573.91	349.94	55.8	59.5	3.73
Waterbodies	4035.9	3619.88	−416.02	43.1	38.6	−4.44
Built-up	55.64	38.46	−17.18	0.6	0.4	−0.18
Barren	53.71	136.97	83.27	0.6	1.5	0.89

emission scenarios (RCP 3.5 to 8.5), for the BoB region, SLR will rise from 0.2 to 1.0 meters in 2100 [68]. At the regional scale, the BoB's sea level is rising by 1.5 mm per year due to global warming [69]. Consequently, the Sundarbans face adverse ecological impacts, particularly on mangrove forest health. Projections by the World Bank [70] estimated that sea levels rising by 10 cm, 25 cm, 45 cm, and 60 cm will submerge 15%, 40%, and 75%, of the entire forest. In another study, 5% of mangrove forest was reduced from 1989 to 2020, and it was forecast that a rise of 1.0 m would abolish the entire Sundarbans [71]. Increasing sea level variations are also linked to climate change and the El Niño Southern Oscillation (ENSO) [72]. Tide Gauge data showed that ENSO and the Indian Ocean Dipole influenced substantial interannual variations in mean sea level [73]. There is a significant association between ENSO events and mangrove mortality [74]. As the surface air and ocean temperatures increase, an exceptional ecosystem and wildlife environment bear considerable threats [75]. Thakur et al. [76] found that NDVI and LST had a negative correlation, with LST being higher over built-up areas, followed by coastlines, mangroves, forests, and waterbodies. Our analysis of LST across various land cover classes concurs with this pattern, as we consistently observed higher LST values over barren areas when compared to mangroves, waterbodies, built-up areas, and other barren lands (see Fig. 9). Our sea-level analysis supports these concerns, with the Sundarbans delta experiencing a cumulative sea-level rise ranging from an average of +17.4 to +1.55 (see Fig. 10), an alarming trend. Besides sea level with associated global warming, some local factors, such as a gentle slope, low elevation, and high tidal amplitude, also contributed to sea-level rise in the Sundarbans [77], except for the Sagar Tidal Gauge. Due to the significant sediment accretion from the Ganges River, Sagar Island has experienced a negative sea level trend [78]. From time to time, built-up is also seen, as well as a large part of it sinking into the seawater or going into the forest. The most significant changes have occurred in the vulnerable southern region, where sea-level rise poses the greatest threat [38]. The waterbodies fluctuated across mangrove forests because the Sundarbans delta crisscrossed many rivers and channels [3], [9], [79].

Simulations from 2030 to 2100 suggest that the Sundarbans mangroves will rapidly disappear in many areas as channels widen and deepen. A combination of satellite observations and simulations reveals that substantial portions of the Sundarbans mangrove forest will become submerged. Water coverage, including all waterways, increased from approximately 3155 km^2 in 1990 to around 4223 km^2 after simulation (see Fig. 11 and Table II). This transformation could be a result of long-term inundation, cyclones, salinity intrusion, and human-induced factors like deforestation [75], [80], [81].

The vulnerability of the Sundarbans region is further exacerbated by its low-lying topography and its historical susceptibility to cyclones [30]. This region experiences cyclones on an annual basis, with a powerful cyclone making landfall approximately every three years [82]. As our climate continues to warm, there is a growing likelihood of intensified cyclogenesis within the BoB, which could result in more frequent and severe cyclones. This, in turn, raises the specter of heightened storm surges, increased inundation, and accelerated coastal erosion. Compounding these concerns is the occurrence of exceptionally high waves along the Bangladesh coast, with a 10-m-high wave emerging roughly every 20 years and a 7-m-high wave appearing approximately once every five years [83]. Moreover, the combination of low coastal topography, a dense population, inadequate coastal protection measures, and the loss of vital vegetation renders the Sundarbans ecosystem exceptionally susceptible to environmental stressors The stark reality of this vulnerability was underscored by the recent impact of two consecutive cyclones, Yaas and Amphan, which wrought significant devastation upon the mangrove forests [80]. These events, coupled with the projections from our future simulations, paint a worrying picture of the worsening condition of the Sundarbans mangrove forest.

In the face of a multifaceted crisis marked by the vanishing mangrove forests, the looming specter of sea-level rise, and the intensification of cyclogenesis, Bangladesh emerges as one of the most profoundly impacted nations by climate change and natural disasters [84]. The ramifications extend to

the jeopardy of food security and livelihoods, with the looming threat of displacing millions [85]. These formidable challenges await planners and local governing bodies in districts compelled to grapple with the inexorable shifts due to climate change [85], [86], [87]. Within this context, both the Governments of Bangladesh and India find themselves at a critical juncture, necessitating the implementation of resolute measures through comprehensive adaptation programs. The crafting of these initiatives can draw valuable insights from the findings of this research, which highlight the intricate interplay of ecological and climatic factors influencing the vulnerability of the region. By incorporating these research-driven insights, policymakers can bolster the effectiveness of their adaptation strategies, enhancing the resilience of vulnerable communities and fortifying their capacity to address the challenges posed by climate change and natural disasters.

V. Conclusion

This article provides a comprehensive analysis of land cover change, vegetation dynamics, LST distribution, sea-level rise, and future land cover change within the Sundarbans delta spanning the period from 1990 to 2100. The CA-ANN simulated model demonstrated commendable performance, achieving an accuracy ranging from 96% to 76%. Notably, the current LULC CA-ANN simulation for the year 2100 revealed a 48% or 4511 km^2 decrease in mangrove coverage. Concurrently, waterbodies exhibited an increase from 3155 to 4223 km^2, alongside expansions in urban and barren areas, reaching 117 and 517 km^2, respectively. However, it is imperative to acknowledge the study's limitations. The identification of only a type of forest, without distinguishing between mangroves and non-mangrove forested areas at a 30-m spatial resolution, poses a constraint on the depth of our findings. Future research endeavors should consider integrating higher-resolution RS data with more classes and within the same neural network-based simulations to enhance the precision of mangrove forest monitoring and management planning. The study highlights a concerning trend of increasing LSTs over the Sundarbans region coupled with a decline in mangrove vegetation. This decline is primarily attributed to natural inundation, driven by sea-level rise a manifestation of the broader impact of global climate change. The Sundarbans mangrove forest has also faced the brunt of several cyclones over the study period, leading to substantial devastation. Encouragingly, our findings indicate that mangrove ecosystems possess a resilience to such natural disturbances, exhibiting the capacity to rebound after a certain period. This article underscores the critical need for ongoing monitoring and adaptive management strategies for the Sundarbans delta. The implications of our study extend beyond the immediate temporal and spatial scope, providing valuable insights into the broader challenges posed by climate change on coastal ecosystems. By emphasizing the limitations, contributions, and implications of our work, we strive to pave the way for future research endeavors aimed at better understanding and safeguarding these ecologically vital regions.

Acknowledgment

We extend our gratitude to the United States Geological Surveyfor providing access to the LULC dataset, which was instrumental in conducting this research. In addition, we would like to express our appreciation to Google for granting us access to the GEE platform, which facilitated our geospatial analyses and enriched the depth of our findings.

References

[1] S. Sarker, A. N. M. S. Huda, M.. N. H. Niloy, and G. W. Chowdhury, "Trophic transfer of microplastics in the aquatic ecosystem of Sundarbans mangrove forest, Bangladesh," *Sci. Total Environ.*, vol. 838, Sep. 2022, Art. no. 155896.

[2] R. Kumar et al., "Microplastics pollution load in Sundarban delta of Bay of Bengal," *J. Hazard. Mater. Adv.*, vol. 7, Aug. 2022, Art. no. 100099.

[3] K. G. Rogers and S. L. Goodbred, "The Sundarbans and Bengal Delta: The world's largest tidal mangrove and delta system," in *Landscapes and Landforms of India*. Berlin, Germany: Springer, 2014, pp. 181–187.

[4] J. Barik and S. Chowdhury, "True mangrove species of Sundarbans delta, West Bengal, eastern India," *Check List*, vol. 10, no. 2, pp. 329–334, 2014.

[5] M. S. Uddin, M. A. R. Shah, S. Khanom, and M. K. Nesha, "Climate change impacts on the Sundarbans mangrove ecosystem services and dependent livelihoods in Bangladesh," *Asian J. Conserv. Biol.*, vol. 2, no. 2, pp. 152–156, 2013.

[6] M.. H. Iqbal, "Valuing ecosystem services of Sundarbans Mangrove forest: Approach of choice experiment," *Glob. Ecol. Conserv.*, vol. 24, Dec. 2020, Art. no. e01273.

[7] S. B. Neogi et al., "Sundarban mangroves: Diversity, ecosystem services and climate change impacts," *Asian J. Med. Biol. Res.*, vol. 2, no. 4, pp. 488–507, Jan. 2017.

[8] M.. S. Uddin, E. D. R. V. Steveninck, M. Stuip, and M. A. R. Shah, "Economic valuation of provisioning and cultural services of a protected mangrove ecosystem: A case study on Sundarbans Reserve Forest, Bangladesh," *Ecosyst. Serv.*, vol. 5, pp. 88–93, Sep. 2013.

[9] M. M. Islam, A. R. Sunny, M. M. Hossain, and D. A. Friess, "Drivers of mangrove ecosystem service change in the Sundarbans of Bangladesh," *Singapore J. Trop. Geogr.*, vol. 39, no. 2, pp. 244–265, 2018.

[10] D. Friess, "Ecosystem Services and Disservices of Mangrove forests: Insights from historical colonial observations," *Forests*, vol. 7, no. 12, Aug. 2016, Art. no. 183.

[11] K. Warren-Rhodes et al., "Mangrove ecosystem services and the potential for carbon revenue programmes in Solomon Islands," *Environ. Conserv.*, vol. 38, no. 4, pp. 485–496, Dec. 2011.

[12] D. N. Wadia, *Geology of India: For Students*. New York, NY, USA: Macmillan, 1919.

[13] J. M. Coleman, "Brahmaputra River: Channel processes and sedimentation," *Sedimentary Geol.*, vol. 3, no. 2–3, pp. 129–239, 1969.

[14] E. J. Bomer, C. A. Wilson, R. P. Hale, A. N. M. Hossain, and F. M. A. Rahman, "Surface elevation and sedimentation dynamics in the Ganges-Brahmaputra tidal delta plain, Bangladesh: Evidence for mangrove adaptation to human-induced tidal amplification," *CATENA*, vol. 187, Apr. 2020, Art. no. 104312.

[15] B. Gopal and M. Chauhan, "Biodiversity and its conservation in the Sundarban mangrove ecosystem," *Aquat. Sci.*, vol. 68, no. 3, pp. 338–354, 2006.

[16] J. F. Richards, "Agricultural impacts in tropical wetlands: Rice paddies for mangroves in South and Southeast Asia," 1990.

[17] P. Chakrabarti, "Evolutionary history of the coastal quaternaries of the Bengal Plain, India," *Proc.-Indian Nat. Sci. Acad. Part A*, vol. 61, pp. 343–354, 1995.

[18] S. M. Islam and M. A. H. Bhuiyan, "Sundarbans mangrove forest of Bangladesh: Causes of degradation and sustainable management options," *Environ., Develop. Sustainability*, vol. 1, no. 2, pp. 113–131, 2018.

[19] X. Zhang, P. M. Treitz, D. Chen, C. Quan, L. Shi, and X. Li, "Mapping mangrove forests using multi-tidal remotely-sensed data and a decision-tree-based procedure," *Int. J. Appl. Earth Observ. Geoinf.*, vol. 62, pp. 201–214, 2017.

[20] M. E. Hoq, "An analysis of fisheries exploitation and management practices in Sundarbans mangrove ecosystem, Bangladesh," *Ocean Coast. Manage.*, vol. 50, no. 5–6, pp. 411–427, 2007.

[21] J. A. Church et al., "'Chapter 13: Sea level change' in Climate Change 2013: The physical science basis: Contribution of Working Group I to the Fifth Assessment Report of the Intergovernmental Panel on Climate Change," 2013, Accessed: Jan. 17, 2024. [Online]. Available: https://digitalcommons.humboldt.edu/hsuslri_state/25/

[22] E. Kristensen, S. Bouillon, T. Dittmar, and C. Marchand, "Organic carbon dynamics in mangrove ecosystems: A review," *Aquatic Botany*, vol. 89, no. 2, pp. 201–219, 2008.

[23] M. Martin, Y. H. Kang, M. Billah, T. Siddiqui, R. Black, and D. Kniveton, "Policy analysis: Climate change and migration Bangladesh," *Dhaka Bangladesh Refug. Migr. Mov. Res. Unit RMMRU*, 2013, Accessed: Jan. 17, 2024. [Online]. Available: http://www.migratingoutofpoverty.org/documents/wp4-ccrm-b-policy.pdf

[24] M. Martin, Y. H. Kang, M. Billah, T. Siddiqui, R. Black, and D. Kniveton, "Climate-influenced migration in Bangladesh: The need for a policy re-alignment," *Develop. Policy Rev.*, vol. 35, no. S2, pp. 357–379, Oct. 2017, doi: 10.1111/dpr.12260.

[25] N. K. Halder, A. Merchant, K. Misbahuzzaman, S. Wagner, and S. A. Mukul, "Why some trees are more vulnerable during catastrophic cyclone events in the Sundarbans mangrove forest of Bangladesh?," *Forest Ecol. Manage.*, vol. 490, Jun. 2021, Art. no. 119117, doi: 10.1016/j.foreco.2021.119117.

[26] J. H. Primavera, "Mangroves, fishponds, and the quest for sustainability," *Science*, vol. 310, no. 5745, pp. 57–59, Oct. 2005, doi: 10.1126/science.1115179.

[27] T. Bucx, M. Marchand, B. Makaske, and C. van de Guchte, "Comparative assessment of the vulnerability and resilience of 10 deltas: Work document," Deltares, Delft-Wageningen, The Netherlands, 2010. Accessed: Jan. 17, 2024. [Online]. Available: https://library.wur.nl/WebQuery/wurpubs/reports/478612

[28] M. Rahman et al., "Temporal dynamics of land use/land cover change and its prediction using CA-ANN model for southwestern coastal Bangladesh," *Environ. Monit. Assessment*, vol. 189, no. 11, pp. 1–18, 2017.

[29] H. M. Prince, M. O. Idrees, H. Z. M. Shafri, M. Iqbal, M. Z. Iqbal, and M. T. Aziz, "Effect of competing landuse practices on Chakaria Sundarbans mangrove in Bangladesh using Landsat imagery," in *Proc. IOP Conf. Ser., Earth Environ. Sci.*, 2018, Art. no. 12038.

[30] S. A. Mukul, S. Huq, J. Herbohn, N. Seddon, and W. F. Laurance, "Saving the Sundarbans from development," *Science*, vol. 368, no. 6496, 2020, Art. no. 1198.

[31] M. S. Chowdhury and B. Hafsa, "Multi-decadal land cover change analysis over Sundarbans Mangrove Forest of Bangladesh: A GIS and remote sensing based approach," *Glob. Ecol. Conserv.*, vol. 37, 2022, Art. no. e02151.

[32] Z. Abbas, G. Yang, Y. Zhong, and Y. Zhao, "Spatiotemporal change analysis and future scenario of LULC using the CA-ANN approach: A case study of the greater bay area, China," *Land*, vol. 10, no. 6, 2021, Art. no. 584.

[33] M. Dede, C. Asdak, and I. Setiawan, "Spatial dynamics model of land use and land cover changes: A comparison of CA, ANN, and ANN-CA," *Register, Jurnal Ilmiah Teknologi Sistem Informasi*, vol. 8, no. 1, pp. 38–49, 2022.

[34] S. Ullah et al., "Remote sensing-based quantification of the relationships between land use land cover changes and surface temperature over the Lower Himalayan Region," *Sustainability*, vol. 11, no. 19, 2019, Art. no. 5492.

[35] S. Abdullah, D. Barua, S. M. A. Abdullah, and Y. W. Rabby, "Investigating the impact of land use/land cover change on present and future land surface temperature (LST) of Chittagong, Bangladesh," *Earth Syst. Environ.*, vol. 6, no. 1, pp. 221–235, 2022.

[36] S. Debanshi and S. Pal, "Wetland delineation simulation and prediction in deltaic landscape," *Ecol. Indicators*, vol. 108, Jan. 2020, Art. no. 105757, doi: 10.1016/j.ecolind.2019.105757.

[37] M. S. Iftekhar and M. R. Islam, "Degeneration of Bangladesh's Sundarbans mangroves: A management issue," *Int. Forestry Rev.*, vol. 6, no. 2, pp. 123–135, 2004.

[38] A. Payo et al., "Projected changes in area of the Sundarban mangrove forest in Bangladesh due to SLR by 2100," *Climatic Change*, vol. 139, pp. 279–291, 2016.

[39] M. K. Ghosh, L. Kumar, and P. K. Langat, "Geospatial modelling of the inundation levels in the Sundarbans mangrove forests due to the impact of sea level rise and identification of affected species and regions," *Geomatics, Natural Hazards Risk*, vol. 10, no. 1, pp. 1028–1046, Jan. 2019, doi: 10.1080/19475705.2018.1564373.

[40] S. N. Islam and A. Gnauck, "Water salinity investigation in the Sundarbans rivers in Bangladesh," *Int. J. Water*, vol. 6, no. 1–2, pp. 74–91, 2011.

[41] H. Mahmood, M. Ahmed, T. Islam, M. Z. Uddin, Z. U. Ahmed, and C. Saha, "Paradigm shift in the management of the Sundarbans mangrove forest of Bangladesh: Issues and challenges," *Trees, Forests People*, vol. 5, Sep. 2021, Art. no. 100094, doi: 10.1016/j.tfp.2021.100094.

[42] USGS, "United States Geological Survey, Landsat 8," 2013. [Online]. Available: https://earthexplorer.usgs.gov/

[43] T. G. Farr et al., "The shuttle radar topography mission," *Rev. Geophys.*, vol. 45, 2007, Art. no. 2.

[44] PSMSL, "Permanent service for mean sea level," 1933. [Online]. Available: https://www.psmsl.org/

[45] S. K. McFeeters, "The use of the Normalized Difference Water Index (NDWI) in the delineation of open water features," *Int. J. Remote Sens.*, vol. 17, no. 7, pp. 1425–1432, 1996.

[46] C. J. Tucker, D. A. Slayback, J. E. Pinzon, S. O. Los, R. B. Myneni, and M. G. Taylor, "Higher northern latitude normalized difference vegetation index and growing season trends from 1982 to 1999," *Int. J. Biometeorol.*, vol. 45, no. 4, pp. 184–190, 2001.

[47] USGS, "Using the USGS Landsat Level-1 data product," 2019. [Online]. Available: https://www.usgs.gov/landsat-missions/using-usgs-landsat-level-1-data-product

[48] G. M. Foody, "Explaining the unsuitability of the kappa coefficient in the assessment and comparison of the accuracy of thematic maps obtained by image classification," *Remote Sens. Environ.*, vol. 239, 2020, Art. no. 111630.

[49] J. A. Sobrino, J. C. Jiménez-Muñoz, and L. Paolini, "Land surface temperature retrieval from LANDSAT TM 5," *Remote Sens. Environ.*, vol. 90, no. 4, pp. 434–440, 2004.

[50] G. Chander, B. L. Markham, and D. L. Helder, "Summary of current radiometric calibration coefficients for Landsat MSS, TM, ETM+, and EO-1 ALI sensors," *Remote Sens. Environ.*, vol. 113, no. 5, pp. 893–903, 2009.

[51] L. Breiman, "Random forests," *Mach. Learn.*, vol. 45, no. 1, pp. 5–32, 2001.

[52] M. Story and R. G. Congalton, "Accuracy assessment: A user's perspective," *Photogramm. Eng. Remote Sens.*, vol. 52, no. 3, pp. 397–399, 1986.

[53] B. Ahmed and A. Dewan, "Application of bivariate and multivariate statistical techniques in landslide susceptibility modeling in Chittagong City Corporation, Bangladesh," *Remote Sens.*, vol. 9, no. 4, pp. 304, 2017.

[54] Z. Hassan et al., "Dynamics of land use and land cover change (LULCC) using geospatial techniques: A case study of Islamabad Pakistan," *SpringerPlus*, vol. 5, no. 1, pp. 1–11, 2016.

[55] H. Ahmad et al., "Evaluation and mapping of predicted future land use changes using hybrid models in a coastal area," *Ecol. Inform.*, vol. 78, 2023, Art. no. 102324, doi: https://doi.org/10.1016/j.ecoinf.2023.102324.

[56] S. Jalayer, A. Sharifi, D. Abbasi-Moghadam, A. Tariq, and S. Qin, "Modeling and predicting land use land cover spatiotemporal changes: A case study in Chalus Watershed, Iran," *IEEE J. Sel. Topics Appl. Earth Observ. Remote Sens.*, vol. 15, pp. 5496–5513, Jul. 2022, doi: 10.1109/JSTARS.2022.3189528.

[57] A. M. Marquez, E. Guevara, and D. Rey, "Hybrid model for forecasting of changes in land use and land cover using satellite techniques," *IEEE J. Sel. Topics Appl. Earth Observ. Remote Sens.*, vol. 12, no. 1, pp. 252–273, Jan. 2019, doi: 10.1109/JSTARS.2018.2885612.

[58] NextGIS, "MOLUSCE—Quick and convenient analysis of land cover changes," 2017. Accessed: Jan. 17, 2024. [Online]. Available: https://nextgis.com/blog/molusce/

[59] Q. D. Team, "QGIS Geographic Information System." QGIS Association, 2022. [Online]. Available: https://www.qgis.org

[60] I. ESRI, "ArcGIS Pro (Version 2.5)," Environmental Systems Research Institute, Redlands, CA, USA, 2020. [Online]. Available: https://www.esri.com/en-us/arcgis/products/arcgis-pro/overview

[61] R. G. Pontius and M. Millones, "Death to Kappa: Birth of quantity disagreement and allocation disagreement for accuracy assessment," *Int. J. Remote Sens.*, vol. 32, no. 15, pp. 4407–4429, 2011, doi: 10.1080/01431161.2011.552923.

[62] T. Lillesand, R. W. Kiefer, and J. Chipman, *Remote Sensing and Image Interpretation*. Hoboken, NJ, USA: Wiley, 2015.

[63] A. O. Amoakoh, P. Aplin, K. T. Awuah, I. Delgado-Fernandez, C. Moses, and C. P. Alonso, "Tropical peatland classification using multi-sensor sentinel imagery and random forest algorithm in Greater Amanzule, Ghana," in *Proc. IEEE Int. Geosci. Remote Sens. Symp.*, 2021, pp. 5910–5913 doi: 10.1109/IGARSS47720.2021.9554615.

[64] S. M. B. Rahaman et al., "Nutrient dynamics in the Sundarbans mangrove estuarine system of Bangladesh under different weather and tidal cycles," *Ecol. Processes*, vol. 2, no. 1, pp. 1–13, 2013.
[65] S. Agarwal, P. Mukherjee, M. Sinha, J. M. Luetz, and A. Mitra, "Anthropogenic Climate change in the Mangrove-dominated Indian Sundarbans: Spatio-temporal analyses, future trends, and recommendations for mitigation and adaptation," in *Climate Change Strategies: Handling the Challenges of Adapting to a Changing Climate*. Berlin, Germany: Springer, 2023, pp. 249–286.
[66] A. K. Paul, R. Ray, A. Kamila, and S. Jana, "Mangrove degradation in the Sundarbans," in *Coastal Wetlands: Alteration and Remediation*. Berlin, Germany: Springer, 2017, pp. 357–392.
[67] S. Robinson, "Climate change adaptation in SIDS: A systematic review of the literature pre and post the IPCC Fifth Assessment Report," *WIREs Clim. Change*, vol. 11, no. 4, Jul. 2020, Art. no. e653, doi: 10.1002/wcc.653.
[68] Y. Hijioka et al., "Asia. In: Climate change 2014: Impacts, adaptation, and vulnerability. Part B: Regional aspects," in *Proc. Contrib. Working Group II 5th Assess. Report Intergovernmental Panel Climate Change*, U.K. and New York, NY, USA, 2014.
[69] N. I. Khan, F. Elahi, and M. A. R. Rana, "A study on the effects of global warming in Bangladesh," *Int. J. Environ. Monit. Anal.*, vol. 3, no. 3, pp. 118–121, 2015.
[70] R. Development, U. South, and A. Region, *Bangladesh Climate Change and Sustainable Development*. Washington, DC, USA: World Bank Group, no. vol. 21104, 2000.
[71] K. Mahadevia Ghimire and M. Vikas, "Climate change–impact on the Sundarbans, a case study," *Int. Sci. J. Environ. Sci.*, vol. 2, no. 1, pp. 7–15, 2012.
[72] C. E. Lovelock et al., "The vulnerability of Indo-Pacific mangrove forests to sea-level rise," *Nature*, vol. 526, no. 7574, pp. 559–563, 2015.
[73] M. Becker et al., "Water level changes, subsidence, and sea level rise in the Ganges–Brahmaputra–Meghna delta," *Proc. Nat. Acad. Sci.*, vol. 117, no. 4, pp. 1867–1876, Jan. 2020, doi: 10.1073/pnas.1912921117.
[74] P. L. Erftemeijer and O. Hamerlynck, "Rufiji Delta (Tanzania) following El Nino floods," Accessed: Jan. 17, 2024. [Online]. Available: https://www.researchgate.net/profile/Olivier-Hamerlynck/publication/262912296_Die-back_of_the_mangrove_Heritiera_littoralis_dryand_in_the_Rufiji_delta_Tanzania_following_El_Nino_floods/links/0f31753928e87828e8000000/Die-back-of-the-mangrove-Heritiera-littoralis-dryand-in-the-Rufiji-delta-Tanzania-following-El-Nino-floods.pdf
[75] A.-A. Jabir, G. M. J. Hasan, and M.. M. Anam, "Correlation between temperature, sea level rise and land loss: An assessment along the Sundarbans coast," *J. King Saud Univ. Eng. Sci.*, pp. S1018363921001136, Aug. 2021, doi: 10.1016/j.jksues.2021.07.012.
[76] S. Thakur et al., "Assessment of changes in land use, land cover, and land surface temperature in the mangrove forest of Sundarbans, northeast coast of India," *Environ. Dev. Sustain.*, vol. 23, no. 2, pp. 1917–1943, 2021, doi: 10.1007/s10668-020-00656-7.
[77] I. Mondal, S. Thakur, P. Ghosh, and T. K. De, "Assessing the impacts of global sea level rise (SLR) on the mangrove forests of Indian Sundarbans using geospatial technology," in *Geographic Information Science For Land Resource Management*. Hoboken, NJ, USA: Wiley, 2021, pp. 209–227.
[78] M. Sahana, S. Rehman, R. Ahmed, and H. Sajjad, "Analyzing climate variability and its effects in Sundarban Biosphere Reserve, India: Reaffirmation from local communities," *Environ. Dev. Sustain.*, vol. 23, no. 2, pp. 2465–2492, Feb. 2021, doi: 10.1007/s10668-020-00682-5.
[79] S. M. Wahid, M. S. Babel, and A. R. Bhuiyan, "Hydrologic monitoring and analysis in the Sundarbans mangrove ecosystem, Bangladesh," *J. Hydrol.*, vol. 332, no. 3–4, pp. 381–395, 2007, doi: 10.1016/j.jhydrol.2006.07.016.
[80] Hindustantimes, "Sunderbans losing its dense mangrove cover: Govt report," Hindustan Times. Accessed: Jan. 17, 2024. [Online]. Available: https://www.hindustantimes.com/India-news/sunderbans-losing-its-dense-mangrove-cover-govt-report-101642099620808.html
[81] M. S. Khan, S. Abdullah, M. A. Salam, T. R. Mandal, and M. R. Hossain, "Review assessment of biodiversity loss of Sundarban forest: Highlights on causes and impacts," *Indonesian J. Forestry Res.*, vol. 8, no. 1, pp. 85–97, 2021.
[82] A. Islam, R. Shaw, and F. Mallick, "Bangladesh Climate Change Strategy and Action Plans," in *Climate Change Adaptation Actions in Bangladesh* (Disaster Risk Reduction), R. Shaw, F. Mallick, and A. Islam, Eds., Tokyo, Japan: Springer, 2013, pp. 107–118. doi: 10.1007/978-4-431-54249-0_7.
[83] S. Dasgupta et al., "Cyclones in a changing climate: The case of Bangladesh," *Clim. Dev.*, vol. 6, no. 2, pp. 96–110, Apr. 2014, doi: 10.1080/17565529.2013.868335.
[84] M. R. Hasan, M. Nasreen, and M. A. Chowdhury, "Gender-inclusive disaster management policy in Bangladesh: A content analysis of national and international regulatory frameworks," *Int. J. Disaster Risk Reduct.*, vol. 41, 2019, Art. no. 101324.
[85] K. F. Davis, A. Bhattachan, P. D'Odorico, and S. Suweis, "A universal model for predicting human migration under climate change: Examining future sea level rise in Bangladesh," *Environ. Res. Lett.*, vol. 13, no. 6, 2018, Art. no. 64030.
[86] M. E. Hauer et al., "Sea-level rise and human migration," *Nature Rev. Earth Environ.*, vol. 1, no. 1, pp. 28–39, 2020.
[87] I. Ahmed et al., "Climate change induced migration: Empirical evidences from the southwest coastal region of Bangladesh," *Int. J. Environ. Sustain. Develop.*, vol. 3, no. 4, pp. 116–126, 2019.

Hafez Ahmad (Fellow, IEEE) was born in Chittagong. He received the bachelor's degree in oceanography from both the University of Chittagong, Chittagong, Bangladesh, and Florida Gulf Coast University, Fort Myers, FL, USA, and the master's degree, in 2024, in wildlife, fisheries, and aquaculture from Mississippi State University, Mississippi State, MS, USA, where he is currently working toward the Ph.D. degree in earth and atmospheric sciences with the Department of Geosciences and the Geosystems Research Institute.

He gained valuable experience working with the Wildlife Conservation Society for a year. His expertise lies in the fields of remote sensing, machine learning, hydrology, and ecological modeling.

Felix Jose received the Master's degree in physical oceanography and the Ph.D degree in marine science both are from the Cochin University of Science & Technology, Kerala, India, in 1993 and 2001, respectively.

He is a Professor of Marine Science and the Chair of the Department of Marine and Earth Sciences, Florida Gulf Coast University, Fort Myers, FL,USA. His expertise is in coastal vulnerability analysis using Hydrodynamic and sediment transport models and remote sensing techniques.

Darren James Shoemaker received the master's degree in biology, in 2021. He is currently working toward the Ph.D. degree in wildlife, fisheries, and aquaculture with the Department of Wildlife, Fisheries and Aquaculture, Mississippi State University, Mississippi State, MS, USA.

His research interests are broad scale predictive modeling of environmental changes under different climate scenarios, primarily focused on aquatic ecosystems.